Title

MAGNETIC ANALYSIS OF ATOMIC AND MOLECULAR BEAMS. I. CONSTRUCTION AND CALIBRATION OF INHOMOGENEOUS DEFLECTING MAGNETS

Authors

Herm, Ronald R.
Herschbach, Dudley R.

Publication Date

1962-10-01

UCRL-10526

University of California

Ernest O. Lawrence Radiation Laboratory

MAGNETIC ANALYSIS OF ATOMIC AND MOLECULAR BEAMS. I. CONSTRUCTION AND CALIBRATION OF INHOMOGENEOUS DEFLECTING MAGNETS

Berkeley, California

DISCLAIMER

UCRL-10526
UC-34 Physics
TID-4500 (18th Ed.)

UNIVERSITY OF CALIFORNIA
Lawrence Radiation Laboratory
Berkeley, California

Contract No. W-7405-eng-48

MAGNETIC ANALYSIS OF ATOMIC AND MOLECULAR BEAMS. I. CONSTRUCTION AND CALIBRATION OF INHOMOGENEOUS DEFLECTING MAGNETS

Ronald R. Herm and Dudley R. Herschbach

October, 1962

Printed in USA. Price $1.00. Available from the
Office of Technical Services
U. S. Department of Commerce
Washington 25, D.C.

MAGNETIC ANALYSIS OF ATOMIC AND MOLECULAR BEAMS. I. CONSTRUCTION AND CALIBRATION OF INHOMOGENEOUS DEFLECTING MAGNETS.*

Ronald R. Herm† and Dudley R. Herschbach

Department of Chemistry and Lawrence Radiation Laboratory, University of California
Berkeley 4, California

Abstract

Three small iron-core electromagnets have been constructed. The overall dimensions of the largest magnet (denoted by A) are about 5" x 5" x 5" and the air gap is 0.10" wide, 0.15" high, 4.5" long. The other magnets (B and C) are shorter and have wider air gaps. The pole tips conform to the cylindrical magnetic equipotential surfaces of the field produced by a pair of infinitely long parallel wires carrying equal and opposite currents. Forty-two turns of 0.18" I.D. copper water tubing carry an energizing current of up to 100 amp which is provided by a transistorized power supply allowing only 0.2% ripple at 100 amps. The efficiency of the magnet design was investigated by measuring the flux through the air gap and various cross sections of the magnet yoke as a function of the energizing current. Magnet A exhibited a peak induction at the midpoint of the gap of about 15 kilogauss, with a transverse gradient of 90 kilogauss/cm. For magnets B and C the peak induction observed was about 10 kilogauss, with a gradient of 30 kilogauss/cm.

---

*Support received from the U. S. Atomic Energy Commission and the Alfred P. Sloan Foundation is gratefully acknowledged.

†National Science Foundation Predoctoral Fellow, 1961-63.

INTRODUCTION

In a magnetic field $\underset{\sim}{H}$, a neutral atom or molecule with magnetic moment $\underset{\sim}{\mu}$ acquires potential energy,

$$W = -\underset{\sim}{\mu} \cdot \underset{\sim}{H} \tag{1}$$

and is accelerated by a force,

$$\underset{\sim}{F} = -\underset{\sim}{\nabla} W. \tag{2}$$

As the only significant dependence of W on position is through the spacial inhomogenity of the field,

$$\underset{\sim}{F} = -\frac{\partial W}{\partial H} \underset{\sim}{\nabla} H. \tag{3}$$

The coefficient $\partial W/\partial H$ differs for each of the $2J + 1$ magnetic substates arising from the various possible orientations of the angular momentum of the molecule, $\underset{\sim}{J}$, and the magnetic field. Thus, if an atomic or molecular beam is sent transversely through an inhomogeneous magnetic field, the beam splits into components corresponding to the various magnetic substates, and each component beam undergoes a deflection determined by the path length and field gradient and by the mass and velocity of the molecules.

The analysis of beams by magnetic deflection is a venerable technique,[1-4] first used in the celebrated Stern-Gerlach

experiment of 1921 which demonstrated the spacial quantization of angular momentum. The aspect most fully exploited has been the selection of magnetic substates, as Rabi developed from this a general method of radiofrequency spectroscopy which has provided hundreds of measurements of nuclear, atomic, and molecular magnetic moments.

In molecular beam scattering experiments, however, there has been little use of magnetic analysis. Three applications of particular interest in this laboratory will be briefly described.

Scattering of magnetically aligned beams. If the electron spins in colliding beams of $J = \frac{1}{2}$ atoms were aligned parallel or antiparallel in successive experiments, a direct comparison of the scattering in the triplet and the singlet states could be made. The intensity limitations do not appear to be prohibitive for beams of alkali metal atoms, for example. The probability of "spin flip" collisions can be studied with one aligned beam.[5] If one of the colliding atoms has $J > \frac{1}{2}$, the dispersion interaction will be noncentral, and the anisotropy of the potential can be studied by use of magnetic analysis; such an experiment has recently been carried out be Berkling, Schlier, and Toschek.[6]

Separation of paramagnetic and diamagnetic species. In crossed beam studies of chemical reactions, such as

$$K + I_2 \longrightarrow I + KI,$$

the detector must distinguish between the elastically scattered K atoms and reactively scattered KI. The most sensitive available detector uses surface ionization on hot filaments, which produces K^+ ions from both K and KI. By comparing readings from filaments which differ in ionization efficiency for K and KI, they can be successfully distinguished, but this method gives somewhat erratic results, especially in regions where the background of elastically scattered K is large.[7] Another approach would be to place a small, strongly inhomogeneous magnet between the scattering center and the detector. This would permit most of the K signal to be "switched on and off" at will, with virtually no effect on the KI signal. In many experiments such a "magnetic filter," might be placed across the exit of a beam oven in order to "purify" the beam. For example, in the reaction

$$K_2 + I \longrightarrow K + KI,$$

the K atoms emitted by the oven would be deflected out and a K_2 beam transmitted by the filter. Magnetic analysis has been used in several beam studies of the dimerization equilibria of alkali atoms, including $2K \rightleftharpoons K_2$, and also in studies of the dissociation equilibria of hydrogen,[9] nitrogen,[9] and fluorine[10] molecules.

Velocity selection. Magnetic deflection of a beam provides velocity analysis as a bonus. Although in practice mechanical selectors usually give better resolution, they

become awkward above about 3×10^5 cm/sec and probably impractical above about 10^6 cm/sec. Thus, magnetic velocity selection is particularly attractive for high temperature beams of light atoms. For example, hydrogen atoms moving at 5×10^6 cm/sec (15 electron volts) will undergo a usable deflection of 0.027 cm on passing through a field 50 cm long with a gradient of 100 kilogauss/cm. An early analysis of magnetic velocity selection was given by Cohen and Ellett,[11] and this has recently been extended by Bederson and Rubin,[12] who are especially concerned with high velocity beams.

This report describes the details of construction and calibration of three small, strongly inhomogeneous magnets (referred to as A, B, and C) to be used in experiments of the sort outlined above. The deflecting power of these magnets is indicated in Fig. 1; however, we shall defer to a subsequent report (Part II of this series) a detailed treatment of the deflection patterns, velocity resolution, and other operational characteristics of the magnets.

MAGNET CONSTRUCTION

A photograph of the largest of the magnets (magnet A, 4.6 inches in length) is shown in Fig. 2.

Pole Tips

The surfaces of the pole tips conform to the "outside" and "inside" of two cylinders differing in radius and axis. As illustrated in Fig. 3, these belong to the family of magnetic

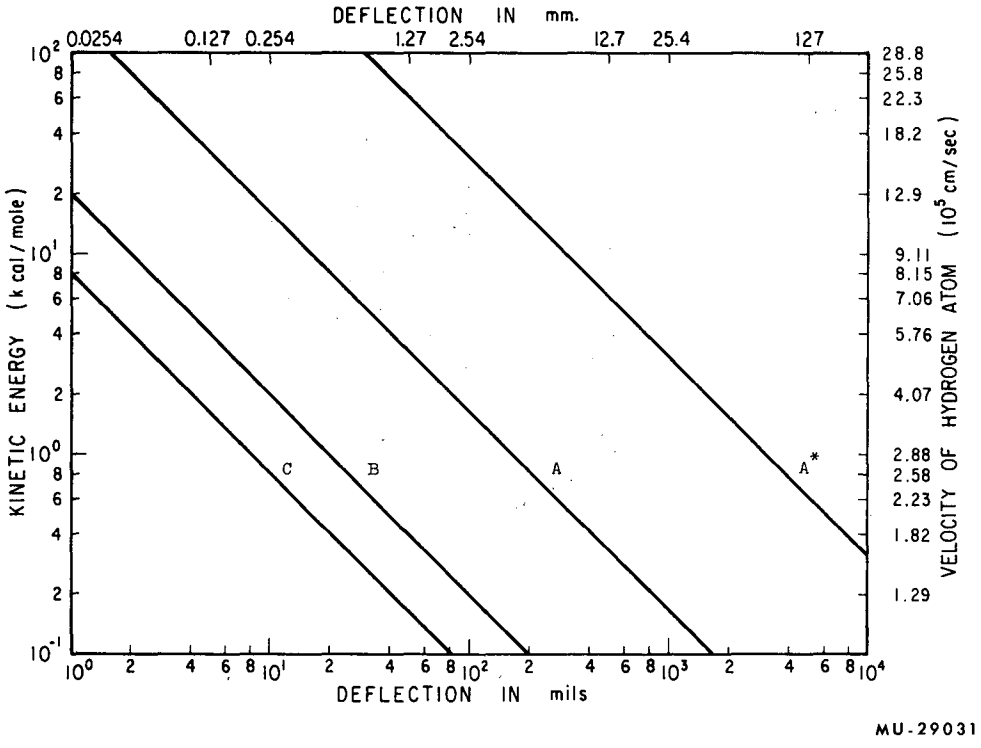

Fig. 1. Deflecting power of magnets (at 100 ampere excitation, see Fig. 13). The hypothetical "magnet A*" is the same as A but 50 cm in length.

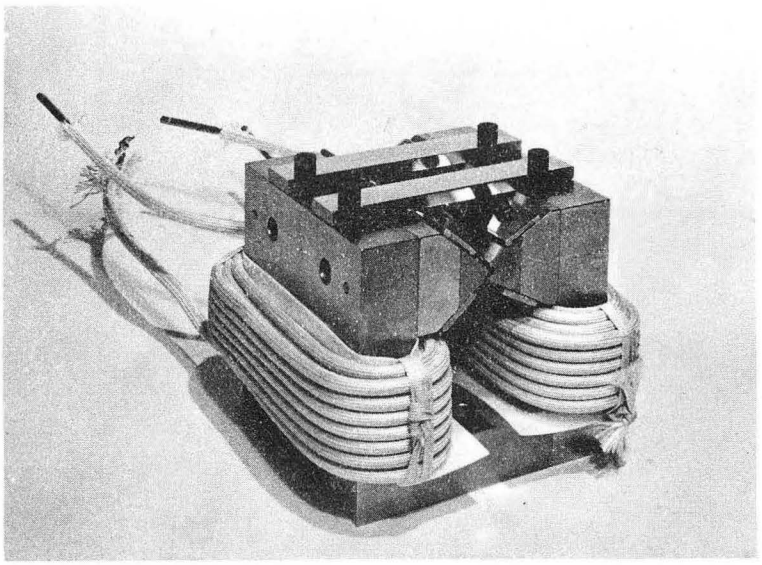

ZN-3452

Fig. 2. Photograph of magnet A. The over-all dimensions of the magnet are about 5"X5"X5".

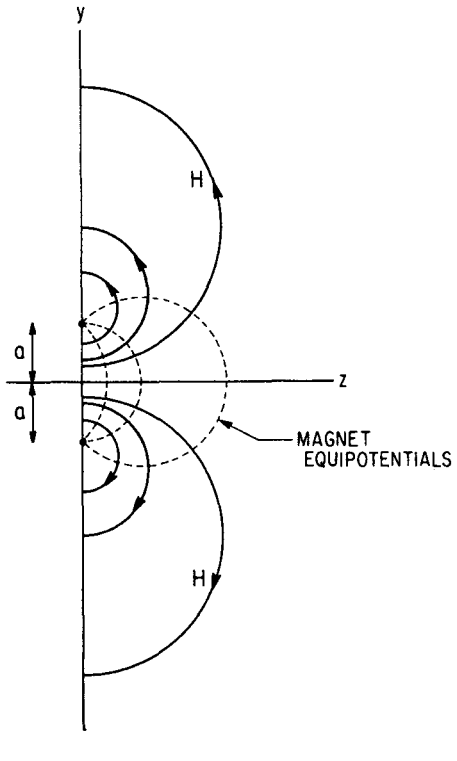

Fig. 3. Magnetic field lines (full curves) and magnetic equipotentials (dashed curves) for two-wire field (after reference 3).

equipotential surfaces of the field produced by two infinitely long parallel conductors of infinitesimal diameter carrying equal but opposite currents. Also shown in Fig. 3 are the lines of magnetic force, which constitute a second, orthogonal family of cylinders.

This "two-wire field, which has become standard for molecular beam deflecting magnets,[3,4] was introduced by Rabi, Kellogg, and Zacharias.[13] As they actually used wires, the field and transverse field gradient at any point could be calculated from the current as[14]

$$H = 2I \frac{2a}{r_1 r_2} \tag{4}$$

and

$$\frac{\partial H}{\partial z} = -2I \frac{2a}{r_1^3 r_2^3} (r_1^2 + r_2^2)\, z, \tag{5}$$

where I is one-tenth the current in amperes and the geometrical quantities are defined in Fig. 4. An advantage of this type of field over that originally used by Stern and Gerlach is that for $z \gtrsim 1.1a$ H and $\partial H/\partial z$ vary only slightly with the coordinate y (parallel to the tall dimension of the beam) between $y = -0.7a$ to $+0.7a$. Thus a tall, ribbon-shaped beam can be used and it will be deflected sideways with very little vertical distortion as long as it does not pass too close to the convex pole tip. Because of the high current densities required, the maximum field attainable with the two-wire arrangement is only about one kilogauss (unless superconducting wire were to be used). Adding iron to the magnetic circuit

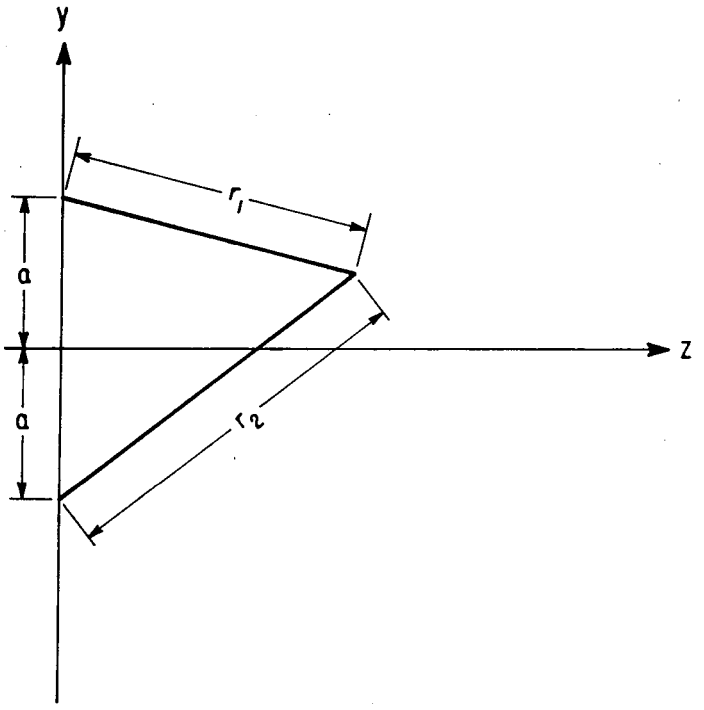

MU-29033

Fig. 4. Definition of coordinate system.

of course leads to much stronger fields; 10-15 kilogauss at saturation is typically obtained.[3,4]

An iron core magnet employing the cylindrical "Rabi pole tips" should produce a field in the air gap with virtually the same families of equipotential surfaces and lines of magnetic force as the equivalent two-wire field. Although it is no longer possible to calculate the field produced by a given energizing current, the ratio of the transverse field gradient to the field is determined solely by geometrical parameters,

$$\frac{\partial H/\partial z}{H} = - \frac{r_1^2 + r_2^2}{r_1^2\, r_2^2}\, z. \tag{6}$$

In the plane $y = 0$,

$$r_1^2 = r_2^2 = a^2 + z^2$$

and

$$\frac{\partial H/\partial z}{H} = - \frac{2z}{a^2 + z^2}\,. \tag{7}$$

Our magnets were designed to give

$$\frac{\partial H/\partial z}{H} \approx 6, \text{ for magnet A}$$

and

$$\frac{\partial H/\partial z}{H} \approx 3, \text{ for magnets B and C}$$

at $z = 1.2a$, the customary beam position. In Table I the ratios calculated from Eq. (7) for $y = 0$ and various values of z are given. Figs. 5 and 6 show the dimensions and relative

Table I. Ratio of transverse gradient to field at $y = 0$.[a]

z/a	$(\partial H/\partial z)/H$ (cm^{-1})	
	Magnet A	Magnets B & C
1.0	-6.29	-3.15
1.1	-6.26	-3.13
1.2	-6.20	-3.10
1.3	-6.08	-3.04
1.4	-5.96	-2.98
1.5	-5.84	-2.98
1.75	-5.44	-2.72
2.0	-5.04	-2.52

[a] $(\partial H/\partial z)/H = -2z/(a^2 + z^2)$; the radius of the convex pole tip is $a = 0.158$ cm for magnet A and $a = 0.317$ cm for magnets B and C.

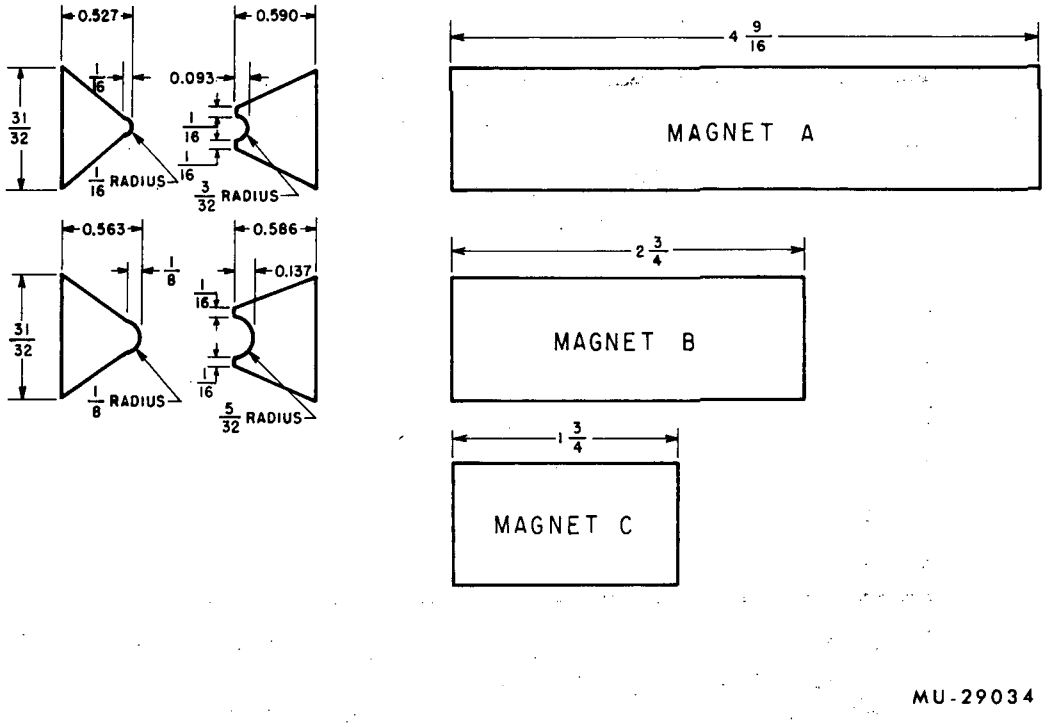

Fig. 5. Dimensions of pole tips.

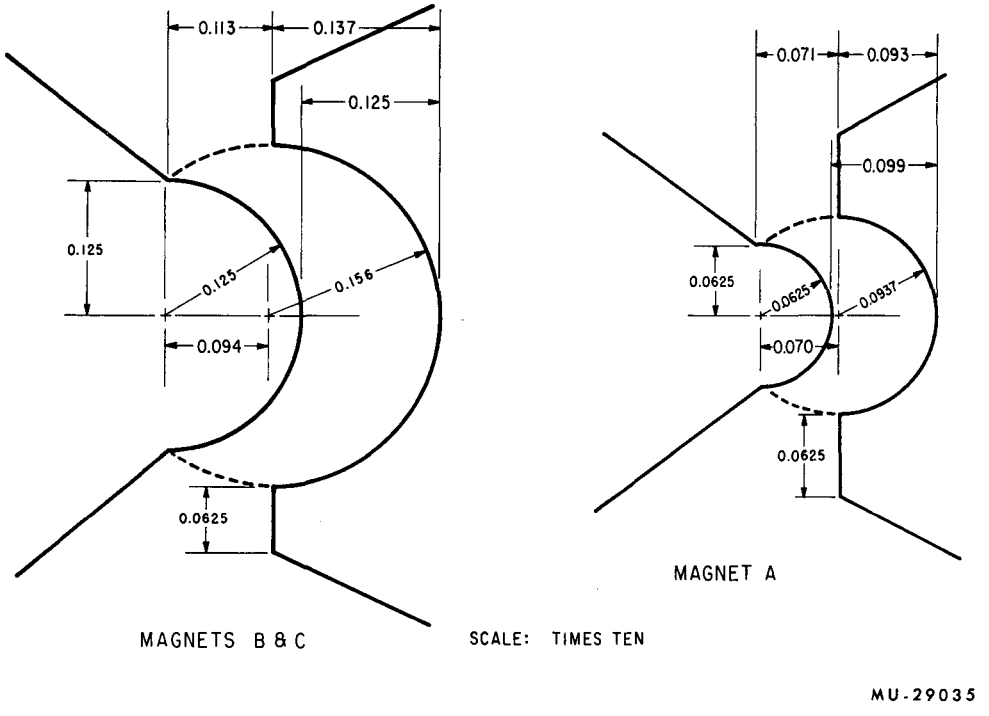

Fig. 6. Relative location of corresponding pole tips.

positions of the pole tips. The tolerance in vertical alignment (y-coordinate) of the pairs of pole tips was less than 0.005". Variations in the horizontal alignment (z-coordinate) were only slightly larger. The maximum width of the air gaps was measured after the final assembly:

For magnet A	0.0990-0.0995"
B	0.1235-0.1245"
C	0.1260-0.1265"

Details of Fabrication

Fig. 7 is an assembly drawing for the magnets, and Table II gives in detail the dimensions of the various parts. The pole tips (parts A and G) are mounted on base pieces (parts B and F) by means of external clamps, and the various sections of the yoke (parts B, C, D, E, F) are bolted together. Braces (shown in Fig. 2) were added to prevent deformation of the yoke. The tips are Western Electric Permendur, the yoke parts are Armco Magnetic Ingot Iron, and the clamps and braces are Stainless Steel. All the iron parts (A to G) were nickel plated to prevent rusting.

The energizing current and cooling water is carried by forty-two turns of 3/16" I.D. copper tubing wound about the yoke, twenty-one turns about each of the sides (parts C and E). Teflon sheet is inserted between the coils and yoke to prevent chafing, and the tubing is insulated with fiberglass sheathing (see Fig. 2).

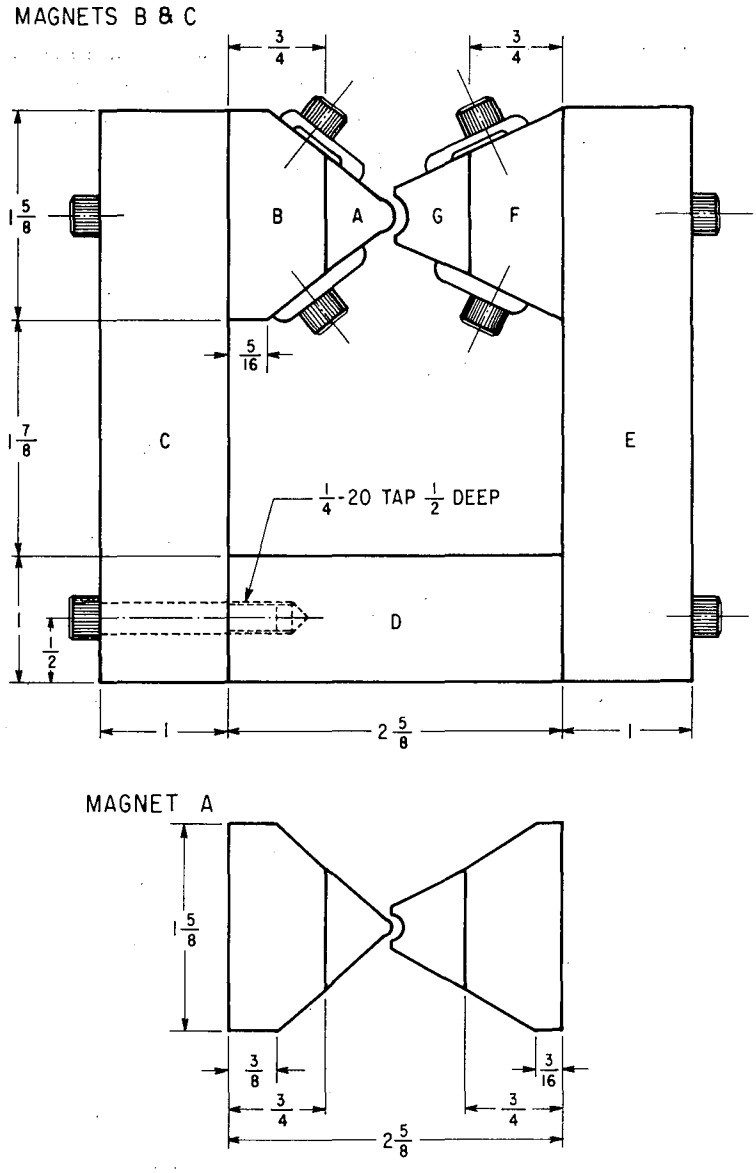

Fig. 7. Assembly drawing for magnets.

Table II. Magnet dimensions (inches).

Dimension	Magnet A	Magnet B	Magnet C
Part A, convex pole tip			
Total Width	0.527	0.563	0.563
Height at Base	31/32	31/32	31/32
Total Length	4-9/16	2-3/4	1-3/4
Radius of Tip	1/16	1/8	1/8
Part B, base for convex tip			
Total Width	3/4	3/4	3/4
Shoulder Width	3/8	5/16	5/16
Height End B-A	31/32	31/32	31/32
Height End C-B	1-5/8	1-5/8	1-5/8
Total Length	4-9/16	2-3/4	1-3/4
Parts C and E, sides of yoke			
Total width	1	1	1
Total Height	4-1/2	4-1/2	4-1/2
Height Bolt to D	1/2	1/2	1/2
Height Bolt to B and F	3-11/16	3-11/16	3-11/16
Total Length	4-9/16	2-3/4	1-3/4
Part D, base of yoke			
Total Width	2-5/8	2-5/8	2-5/8
Total Height	1	1	1
Total Length	4-9/16	2-3/4	1-3/4
Part F, base of concave tip			
Total Width	3/4	3/4	3/4
Shoulder Width	3/16	0	0
Height End E-F	1-5/8	1-5/8	1-5/8
Height End F-G	31/32	31/32	31/32
Total Length	4-9/16	2-3/4	1-3/4
Part G, concave pole tip			
Total Width	0.590	0.586	0.586
Width Groove	0.093	0.137	0.137
Height Base	31/32	31/32	31/32
Height Shoulders	1/16	1/16	1/16
Total Length	4-9/16	2-3/4	1-3/4
Radius Groove	3/32	5/32	5/32

Power Supply

The energizing current is furnished by a transistorized, regulated DC power supply capable of delivering 0-100 amps at 0-10 volts.[15] Tests of the supply show it allows ripple of 0.15 amps RMS, short term fluctuations of one part in 10^5, and long term fluctuations of one to five parts in 10^4 over one-half to one hour.

METHOD OF CALIBRATION

A search coil technique was used to measure the flux through various regions of the magnetic circuit. The principles involved are well-known, but will be reviewed briefly. The flux through a coil composed of N loops of wire which enclose an area A is

$$\Phi = NAB, \tag{8}$$

where B denotes the component of the magnetic induction normal to the area of the coil. B is assumed to be constant over the coil. A change in the flux induces an EMF given by

$$E = -\frac{d\Phi}{dt},$$

and therefore

$$-\frac{dB}{dt} = \frac{E}{NA} = \frac{Ri}{NA} = \frac{R}{NA}\frac{dQ}{dt}, \tag{9}$$

where R is a standard resistance in series with the induced EMF, i is the current in R, and Q is the charge developed across a capacitor C in series with R. If the polarity of the field is reversed during the time interval τ,

$$\int_0^{\tau} (-dB/dt)dt = -\int_{-B}^{B} dB = (R/NA)\int_0^{Q} dQ$$

$$2B = -(R/NA)Q$$

or

$$B = -\frac{RC}{2NA}V \tag{10}$$

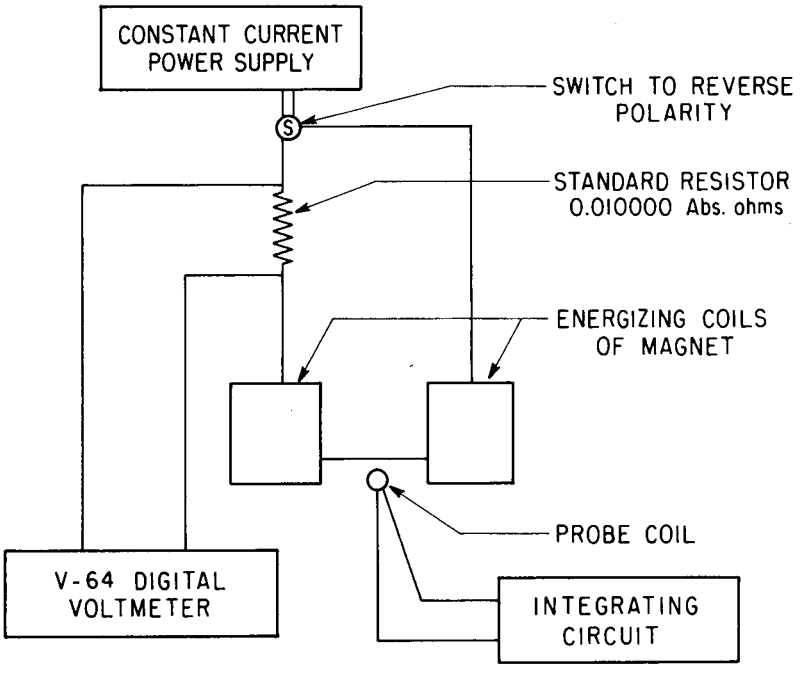

Fig. 8. Schematic diagram of circuit employed in field measurements.

where V is the voltage developed across the capacitance as a consequence of the integrated EMF.

Diagrams of the actual circuits employed are given in Figs. 8 and 9. Search coils were placed about various parts of the magnet and the normal component of the magnetic induction in each coil was determined as a function of the energizing current supplied to the magnet. B was evaluated from Eq. (10) by measuring the voltage V developed in the integrating circuit of Fig. 9 when the polarity of the energizing current was reversed. The energizing current was determined from the IR drop across an oil-cooled resistance (0.010000 absolute ohms) in series with the magnet coils.

Figure 10 shows the positions of the various search coils. The coils were made of 0.0054" diameter copper wire. The area of any of the coils about the iron core was taken as the cross-sectional area of the core at the position of the coil. The dimensions of the search coils used in the air gap are shown in Fig. 11. These coils were securely fixed with respect to the air gap boundaries by means of plastic spacers, as indicated in Fig. 12. The area of each search coil used in the air gap was measured in an auxiliary experiment employing a homogeneous permanent magnetic field. The voltage V_s developed in the integrating circuit when the search coil was rotated through 180° in this field was measured, and compared with the voltage V_0 produced by rotating a standard coil of known area, A_0. The area of the search coil was then taken as

$$A = (V_s/V_0)\, A_0.$$

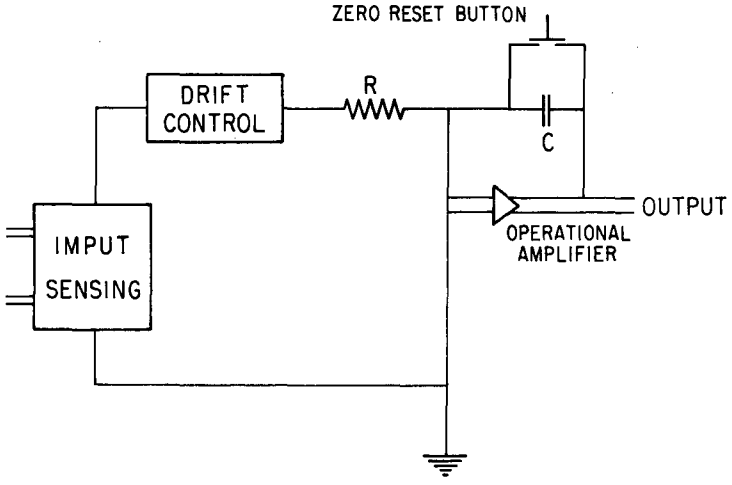

Fig. 9. Schematic diagram of integrating circuit. R and C are variable. The drift control compensates for thermal EMF's; the zero reset discharges the capacitor; the input switch selects the source and polarity of the input signal.

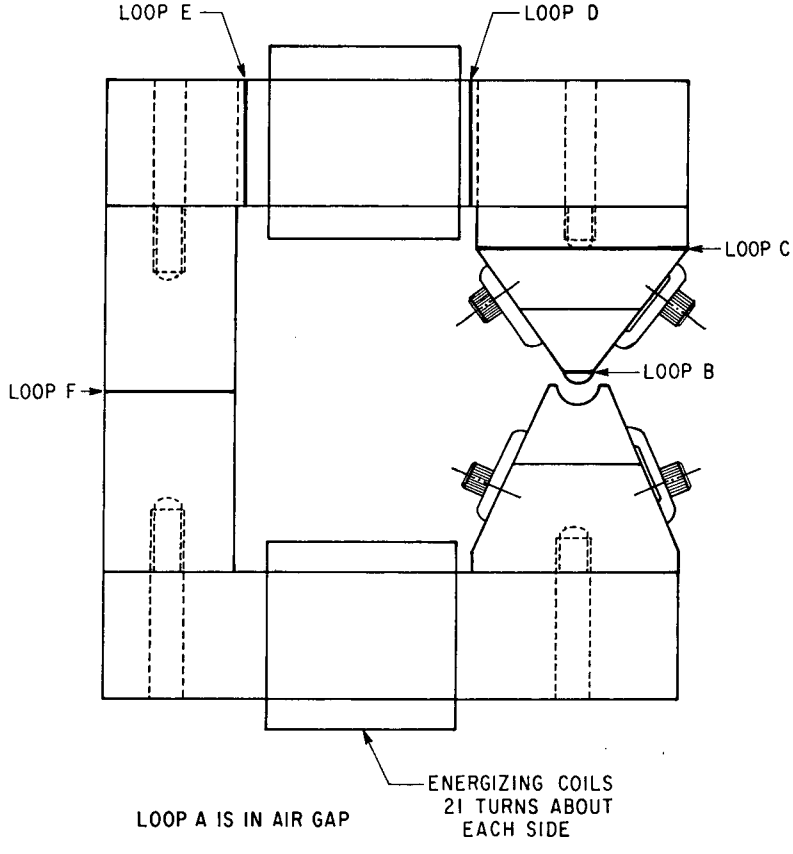

Fig. 10. Location of search coils.

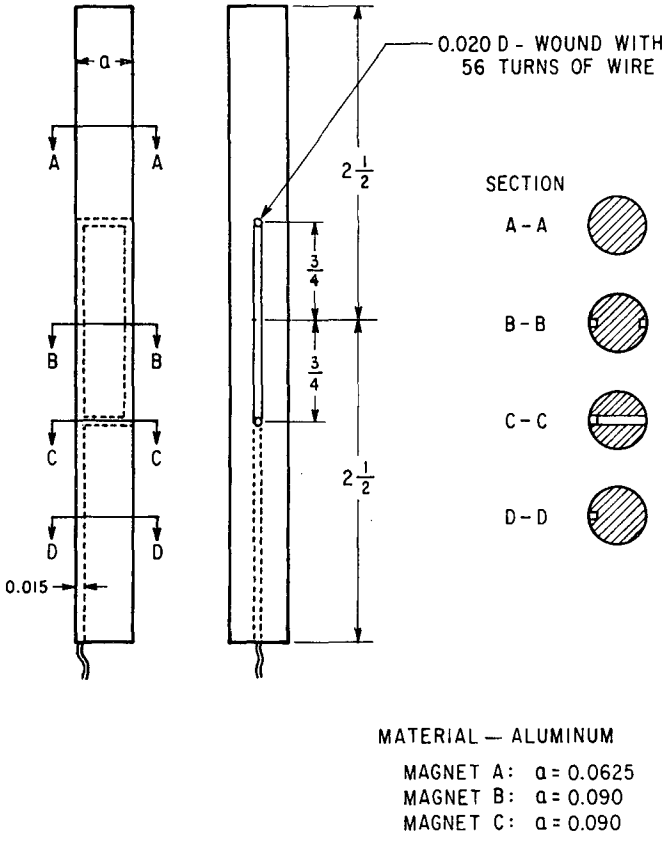

Fig. 11. Dimensions of search coils used in the air gaps.

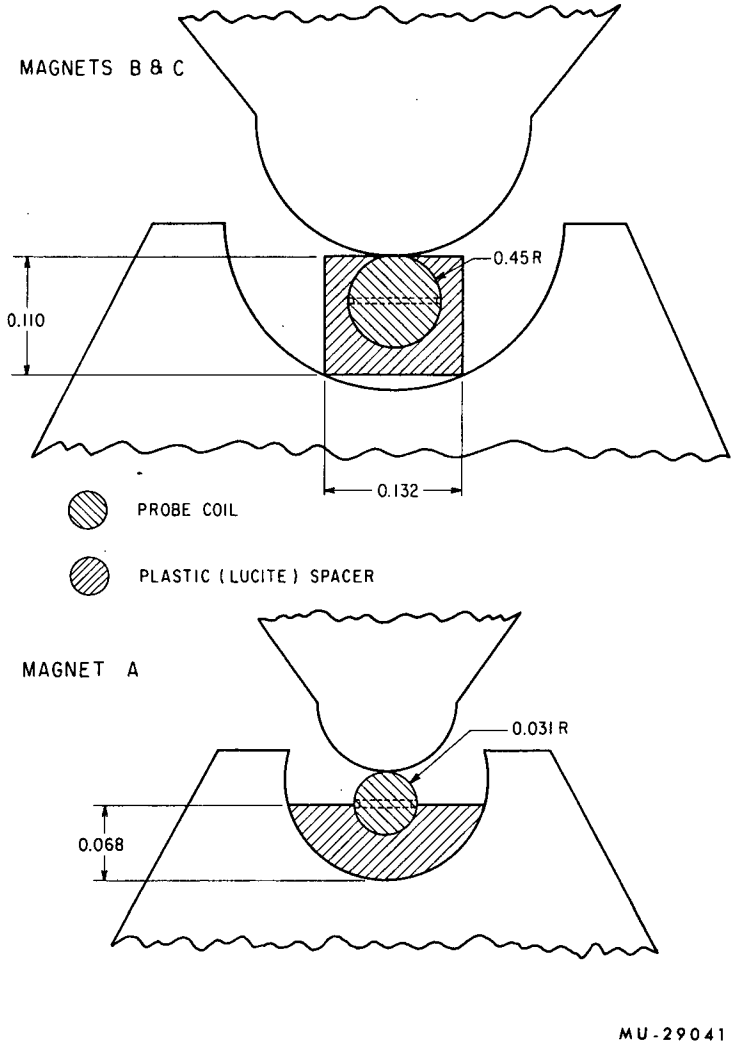

Fig. 12. Location of search coils relative to gap boundaries.

RESULTS OF CALIBRATIONS

Figures 13-16 summarize the search coil measurements. It is seen that within the air gap fields of 15 kilogauss are readily accessible in magnet A, and 10 kilogauss in magnets B and C. According to Table I, these fields produce transverse gradients of about 90 kilogauss/cm for magnet A and 30 kilogauss/cm for magnets B and C. All three magnets are approaching saturation as the energizing current nears 100 amperes. As indicated in Figs. 14-16, the saturation appears to occur close to the pole tips, where the cross-section of the core necessarily becomes rather small, and thus the dimensions chosen for the magnet yoke are satisfactory.

The accuracy of the calibration curves, especially for the air gap region (Fig. 13), is probably not better than ±5%. However, this is quite sufficient for the applications which are planned.

Since we may regard the field within the air gap as defined by the equipotentials and lines of force for the equivalent two-wire field, the experimentally measured B can be related to the parameter I in Eqs. (4) and (5). Thus, although Fig. 13 refers to the midpoint of the search coil ($y = 0$, $z = 1.3a$), the field and gradient at any other point within the air gap are easily obtained by substituting into Eqs. (4) and (5)

$$I = 0.106B, \text{ for magnet A;} \tag{11a}$$

or

$$I = 0.212B, \text{ for magnets B and C,} \qquad (11b)$$

where the value of B corresponding to the energizing current used is taken from Fig. 13.

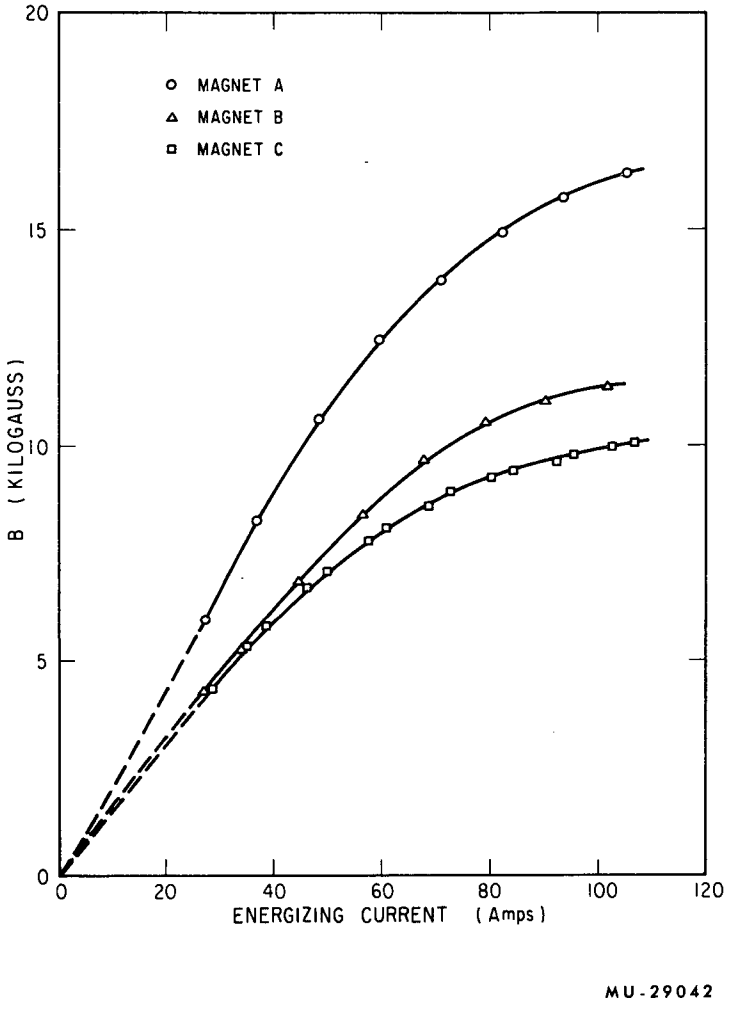

Fig. 13. Magnetic induction in the air gap versus energizing current, for magnets A, B, C.

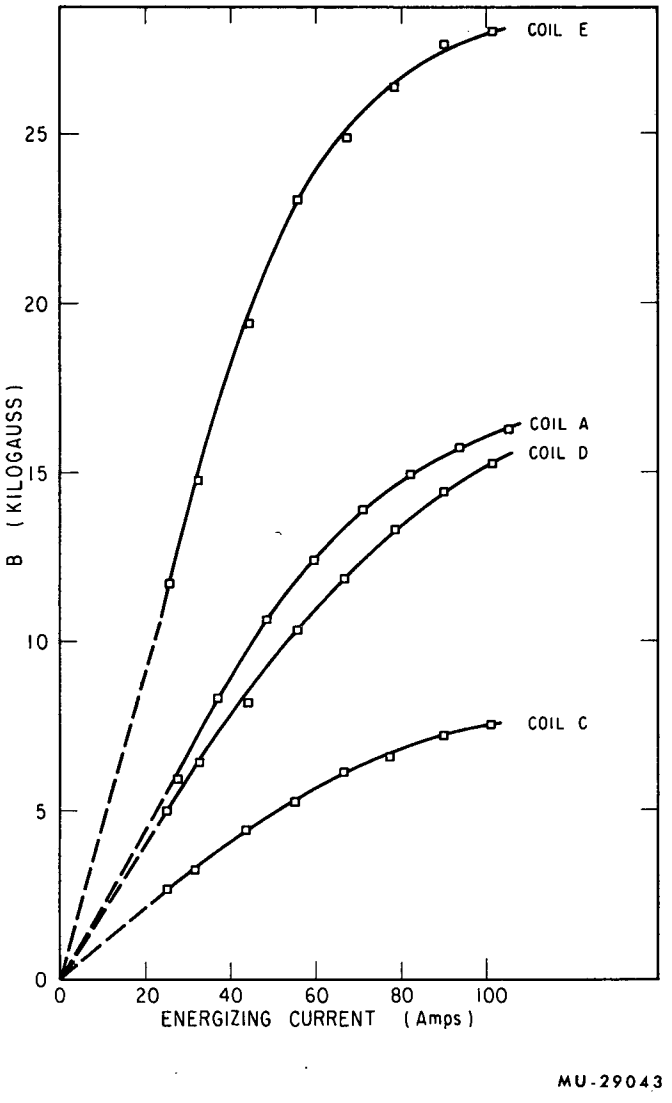

Fig. 14. Magnetic induction through magnet A versus energizing current, for various search coil positions (see Fig. 10).

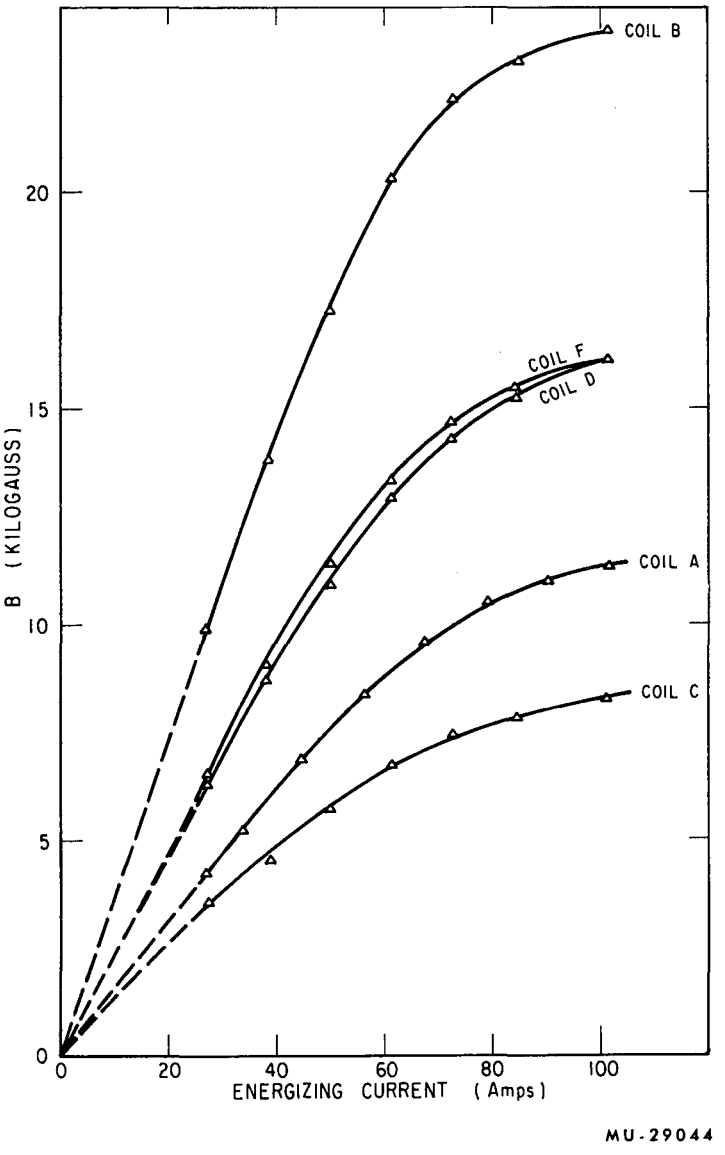

Fig. 15. Magnetic induction through magnet B versus energizing current, for various search coil positions (see Fig. 10).

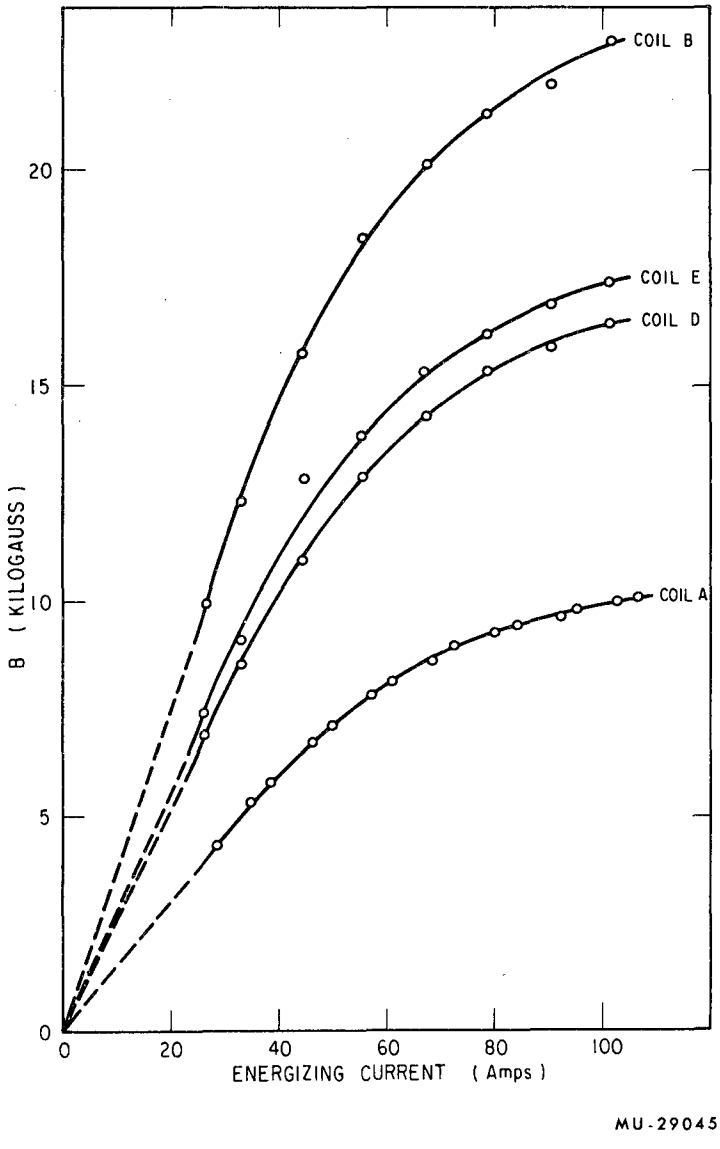

Fig. 16. Magnetic induction through magnet C versus energizing current, for various search coil positions (see Fig. 10).

APPENDIX

Average of Flux Over Coil Area

Other methods[16,17] of calibrating the field within the air gap would probably be preferable to that used here if greater accuracy were required. Nonetheless, it may be worthwhile to indicate an improvement that could be made in the analysis of the search coil measurements. To make this refinement significant, it would be necessary to fix the position of the search coil within the gap more accurately than in our measurements, but this could be done by means of properly machined brass spacers.

In deriving Eq. (10), our main assumptions were (a) that the lines of magnetic induction crossing the area of the search coil are all mutually parallel and (b) that the normal component B is constant over the coil. For a coil located in the strongly inhomogeneous field of the air gap these assumptions are clearly much more approximate than for coils about the iron core. For the air gap Eq. (8) should be replaced by

$$\Phi = NA\overline{B} \tag{12}$$

where $\overline{B}$ denotes a suitable average, over the search coil area, of the variations in direction and magnitude of the induction. The experimental B obtained in Eq. (10) and Fig. 13 likewise should be properly interpreted as $\overline{B}$. The average may be evaluated from the spatial variation of the two-wire field prescribed by Eq. (4). The calculation will therefore yield a

relation between I and $\bar{B}$ which should provide a more accurate prediction of the air gap field than given by Eq. (11).

The notation used is shown in Fig. 17. The two-wire equipotentials constitute a family of circles which all pass through the points $(y = a,\ z = 0)$ and $(y = -a,\ z = 0)$. The search coil is located symmetrically with respect to the plane $y = 0$. It has negligibly small thickness, width 2b, and lies in the plane $z = a + d$, at distance d from the convex pole tip. There is an equipotential intersecting both of the endpoints of the coil, $(b, a + d)$ and $(-b, a + d)$. The radius r and origin $(0,h)$ of this equipotential may be determined from

$$a^2 + h^2 = r^2 \tag{13}$$

and

$$b^2 + (a + d - h)^2 = r^2.$$

The flux through the search coil is that cutting this circle between $-\theta_o$ to $+\theta_o$, where

$$\theta_o = \arcsin (b/r). \tag{14}$$

Furthermore, the flux lines are all normal to the equipotential surface. Therefore, the total flux through the coil is

$$\Phi = \int_{-\theta_o}^{\theta_o} d\Phi = N \int_{o}^{\ell} \int_{-\theta_o}^{\theta_o} B(\theta) dA, \tag{15}$$

where ℓ is the length of the search coil and

$$B(\theta) = H(\theta) = 4aI/r_1 r_2$$

$$dA = r d\theta d\ell.$$

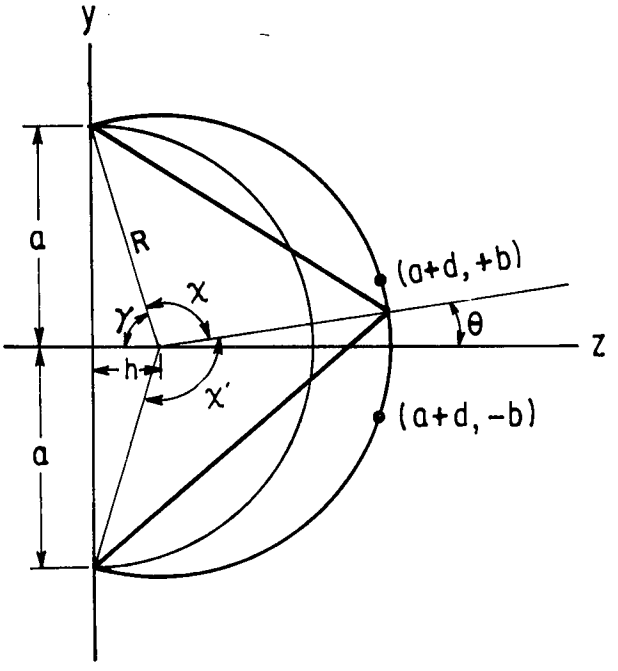

MU-29046

Fig. 17. Definition of coordinates used in averaging flux over search coil area.

Accordingly,

$$\Phi = 4NIar\ell \int_{-\theta_o}^{\theta_o} \frac{d\theta}{r_1 r_2} = 8NIar\ell \int_{0}^{\theta_o} \frac{d\theta}{r_1 r_2} , \tag{16}$$

and, on comparing Eq. (12), we obtain

$$I = F(\theta_o)\bar{B} , \tag{17}$$

where

$$F(\theta_o) = b/\left(4ar \int_{0}^{\theta_o} \frac{d\theta}{r_1 r_2}\right). \tag{18}$$

To evaluate the factor $F(\theta_o)$, we require r_1 and r_2 as functions of θ. From Fig. 17,

$$r_1^2 = 2r^2(1-\cos\chi) \tag{19}$$

$$r_2^2 = 2r^2(1-\cos\chi')$$

and if we define

$$\gamma = \arcsin\,(a/r) \tag{20}$$

then

$$\begin{aligned} \chi &= \pi-\gamma-\theta \\ \chi' &= \pi-\gamma+\theta \end{aligned} \tag{21}$$

In general, Eq. (18) must be evaluated numerically. If the width of the search coil becomes negligible,

$$\theta_o \longrightarrow 0,$$

$$F(\theta_o) \longrightarrow \frac{a^2+(a+d)^2}{4a} , \tag{22}$$

and Eq. (17) reduces to Eq. (11).

ACKNOWLEDGMENTS

We wish to thank Carl Baugh for his skilful workmanship in the fabrication of the magnets. We are also much indebted to our colleague, John Birely, and to Joseph Dorst, Peter Watson, and Fred Macondray of the Magnet Testing Group, for their assistance and advice in the calibrations.

References

1. R. G. J. Fraser, Molecular Rays (Cambridge University Press, 1931).
2. K. F. Smith, Molecular Beams (Methuen Monographs, 1955).
3. N. F. Ramsey, Molecular Beams (Clarendon Press, Oxford, 1956).
4. P. Kusch and V. Hughes, Handbuch der Physik, 37 (Springer, 1959).
5. K. Rubin, J. Perel, and B. Bederson, Phys. Rev. 117, 151 (1960).
6. K. Berkling, C. Schlier, and P. Toschek, Zeitschrift f. Physik, 168, 81 (1962).
7. D. R. Herschbach, Disc. Faraday Soc. 33 (1962).
8. L. C. Lewis, Zeitschift f. Physik, 69, 786 (1931).
9. J. M. Hendrie, J. Chem. Phys. 22, 1503 (1954).
10. T. A. Milne and P. W. Gilles, J. Am. Chem. Soc. 81, 6115 (1959).
11. V. W. Cohen and A. Ellett, Phys. Rev. 51, 65 (1937).
12. B. Bederson and K. Rubin, AEC Technical Report NYO-10, 117 (New York University, New York, February, 1962).
13. I. I. Rabi, J. M. B. Kellogg, and J. R. Zacharias, Phys. Rev. 46, 157 (1934).
14. Reference 3, pp. 398, 431-432.
15. Electronic Measurements Company, Red Bank, Eatontown, New Jersey.
16. Reference 1, p. 116-117.
17. R. M. Bozorth, Rev. Mod. Phys. 19, 29 (1947).